

Supplementary Materials:

Maurizio Manigrasso¹, Giulia Simonetti², Maria Luisa Astolfi², Cinzia Perrino³, Silvia Canepari², Carmela Protano⁴, Arianna Antonucci⁴, Pasquale Avino⁵, Matteo Vitali^{4*}

¹ Department of Technological Innovations, INAIL, Via Roberto Ferruzzi 38, 00143 Rome, Italy; m.manigrasso@inail.it

² Chemistry Department, Sapienza University of Rome, P.le Aldo Moro 5, 00185 Rome, Italy; giulia.simonetti@uniroma1.it; marialuisa.astolfi@uniroma1.it; silvia.canepari@uniroma1.it

³ C.N.R. Institute of Atmospheric Pollution Research, Via Salaria , km 29, 300, Monterotondo St., 00015 Rome, Italy; perrino@iaa.cnr.it

⁴ Department of Public Health and Infectious Diseases, Sapienza University of Rome, P.le Aldo Moro 5, 00185 Rome, Italy; carmela.protano@uniroma1.it; matteo.vitali@uniroma1.it

⁵ Department of Agricultural, Environmental and Food Sciences (DiAAA), University of Molise, 86100 Campobasso, Italy; avino@unimol.it

* Correspondence: matteo.vitali@uniroma1.it

Supplementary material S1: Analytical procedures for OP assays

DTT assay

0.7 mLs of water extract were incubated with DTT (Sigma, Zwijndrecht). The reaction was stopped at designated time (0, 5, 10, 15, 20 min), by adding 1 mL of trichloroacetic acid 10%. 1 mL of each solution was then mixed with 2 mL of Tris-buffer (0.08M, containing EDTA 4 mM) and with 50 µL of 0.2 mM 5,50-dithiobis-2-nitrobenzoic acid (DTNB, Sigma, Zwijndrecht). The absorbance at 412 nm was recorded; the results are expressed as nmol DTT min⁻¹ per sampled volume (m³) or per mg of PM. Domestic oil burning furnace (DOFA, obtained from US EPA, RTP, NC) with a fixed concentration was used as a positive control and ultrapure water as a negative control.

AA assay

PM extracts are incubated in the spectrophotometer (spectra MAX 190: Molecular Devices, Sunnyvale, USA) for 10 min at 37 °C. After adding ascorbate acid, the absorption at 265 nm is measured at designated time (0, 5, 10, 15, 20 min). The maximum depletion rate of ascorbic acid is determined by linear regression of the linear section data, plotted as absorbance against time. Domestic oil burning furnace (DOFA obtained from US EPA, RTP, NC) with a fixed concentration was used as a positive control and ultrapure water as a negative control.

DCFH assay

The DCFH-DA solutions were prepared by dissolving 4.873 mg of the reagent in 5mL of CH₃CH₂OH in the dark. Then, 20 mL NaOH 0.01M were added to favour the de-acetalization reaction; the solution was then kept in the dark at room temperature for 30 minutes before use. The HRP solution (0.5 units/mL) was prepared by dissolving proper weighted amount of the commercial product (Type VI, essentially salt-free, lyophilized powder, ≥250 units/mg solid) in 1L of 25 mM phosphate buffer at pH 7.4 and incubated at 37 °C for 15 minutes. Sample's water extracts (1.5 mL) and 5 µM DCFH (125 µL) were added to 5 mL of the buffered HRP solution and the solution was kept at 37°C for 15 min. The intensity of the fluorescence radiation at 530 nm was then measured by a Fluorescence detector (Jasco FP-920; excitation wavelength: 427 nm). The calibration curve was obtained daily by standard H₂O₂ solutions (5x10⁻⁶, 1×10⁻⁷, 2×10⁻⁷, 5x10⁻⁷, 1x10⁻⁶ M) and the measured fluorescence intensity was converted into equivalent H₂O₂ concentrations.

Limits of detection (LODs), Limits of quantification (LOQs), calculated by following the IUPAC (International Union of Pure and Applied Chemistry) indications as three times and ten times the standard deviation of the blank, respectively (10 replicates) and repeatability (R%), determined by

evaluating the mean relative repeatability of paired samples as indicated by UNI EN14902, of the OP assays are reported in the following table:

	R _{REL} %	LOD	LOQ
DCFH	2.5	0.7 nM _{H2O2}	8 nM _{H2O2}
DTT	4.4	0.09 nMmin ⁻¹	0.3 nMmin ⁻¹
AA	7.6	0.2 nMmin ⁻¹	0.8 nMmin ⁻¹

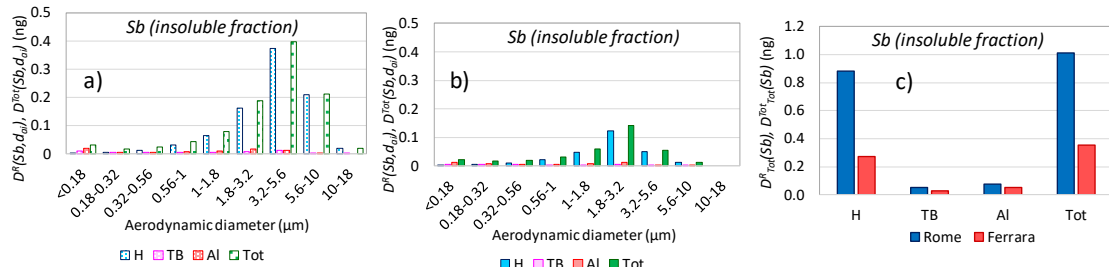


Figure S1. $D^R(Sb, d_{ai})$ and $D^{Tot}(Sb, d_{ai})$ doses at the Rome (a) and Ferrara (b) sites, relevant $D^R_{Tot}(Sb)$ and $D^{Tot}_{Tot}(Sb)$ doses (c) for Sb insoluble fraction.

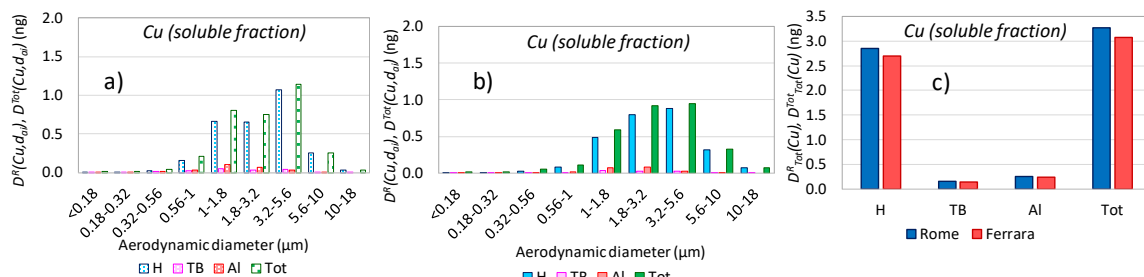


Figure S2. $D^R(Cu, d_{ai})$ and $D^{Tot}(Cu, d_{ai})$ doses at the Rome (a) and Ferrara (b) sites, relevant $D^R_{Tot}(Cu)$ and $D^{Tot}_{Tot}(Cu)$ doses (c) for Cu soluble fraction.

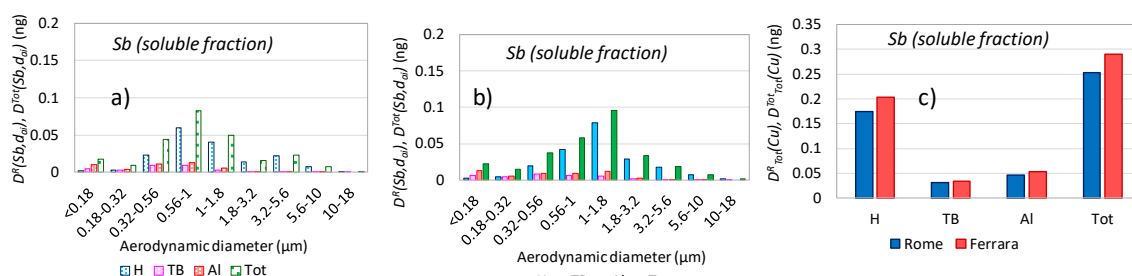


Figure S3. $D^R(Sb, d_{ai})$ and $D^{Tot}(Sb, d_{ai})$ doses at the Rome (a) and Ferrara (b) sites, relevant $D^R_{Tot}(Sb)$ and $D^{Tot}_{Tot}(Sb)$ doses (c) for Sb soluble fraction.

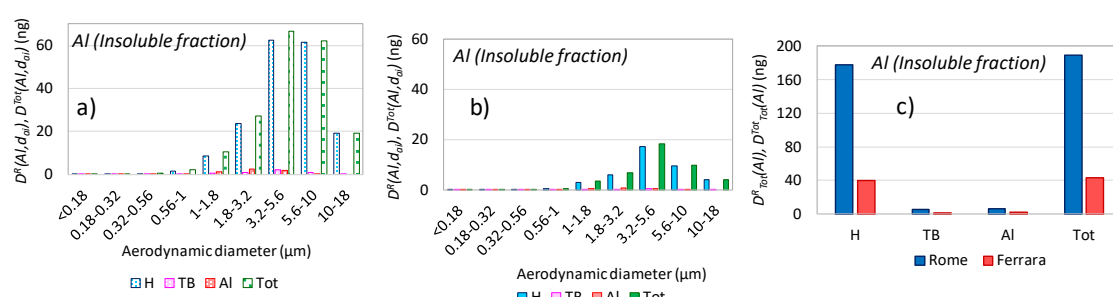


Figure S4. $D^R(Al, d_{ai})$ and $D^{Tot}(Al, d_{ai})$ doses at the Rome (a) and Ferrara (b) sites, relevant $D^R_{Tot}(Al)$ and $D^{Tot}_{Tot}(Al)$ doses (c) for Al insoluble fraction.

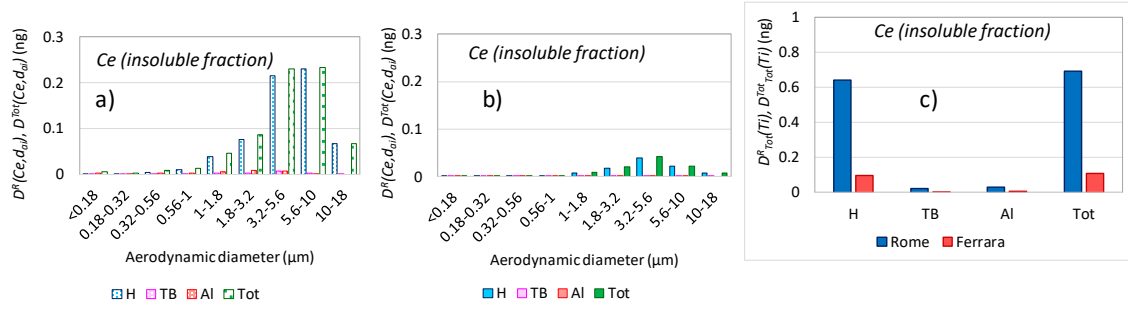


Figure S5. $D^R(Ce, d_{ai})$ and $D^{Tot}(Ce, d_{ai})$ doses at the Rome (a) and Ferrara (b) sites, relevant $D^R_{Tot}(Ce)$ and $D^{Tot}_{Tot}(Ce)$ doses (c) for Ce insoluble fraction.

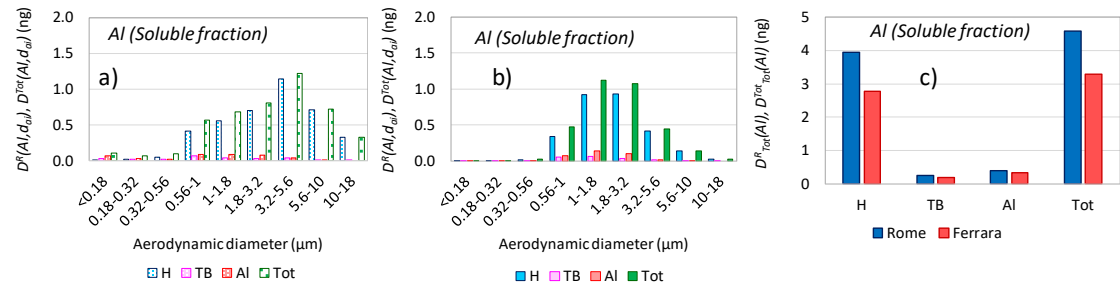


Figure S6. $D^R(Al, d_{ai})$ and $D^{Tot}(Al, d_{ai})$ doses at the Rome (a) and Ferrara (b) sites, relevant $D^R_{Tot}(Al)$ and $D^{Tot}_{Tot}(Al)$ doses (c) for Al soluble fraction.

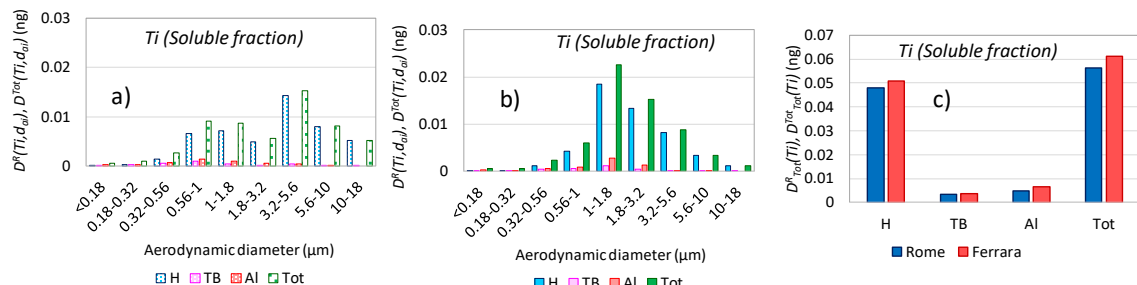


Figure S7. $D^R(Ti, d_{ai})$ and $D^{Tot}(Ti, d_{ai})$ doses at the Rome (a) and Ferrara (b) sites, relevant $D^R_{Tot}(Ti)$ and $D^{Tot}_{Tot}(Ti)$ doses (c) for Ti soluble fraction.

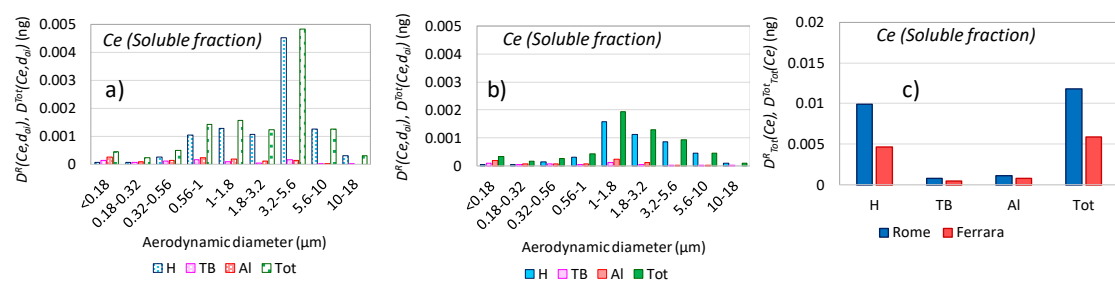


Figure S8. $D^R(Ce, d_{ai})$ and $D^{Tot}(Ce, d_{ai})$ doses at the Rome (a) and Ferrara (b) sites, relevant $D^R_{Tot}(Ce)$ and $D^{Tot}_{Tot}(Ce)$ doses (c) for Ce soluble fraction.

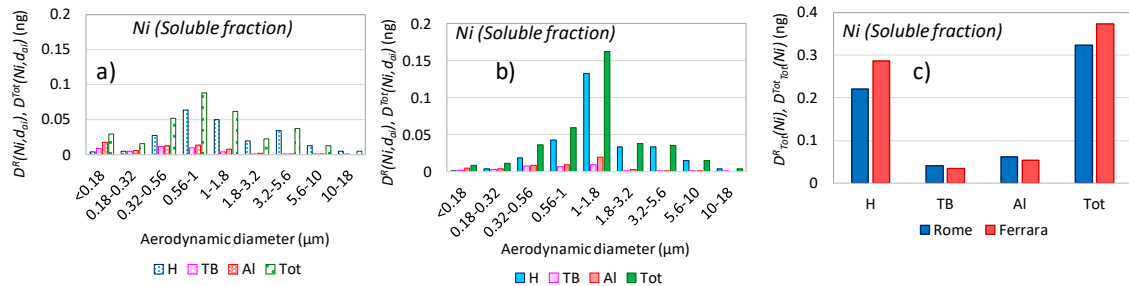


Figure S9. $D^R(Ni, d_{ai})$ and $D^{Tot}(Ni, d_{ai})$ doses at the Rome (a) and Ferrara (b) sites, relevant $D_{Tot}^R(Ni)$ and $D_{Tot}^{Tot}(Ni)$ doses (c) for Ni soluble fraction.

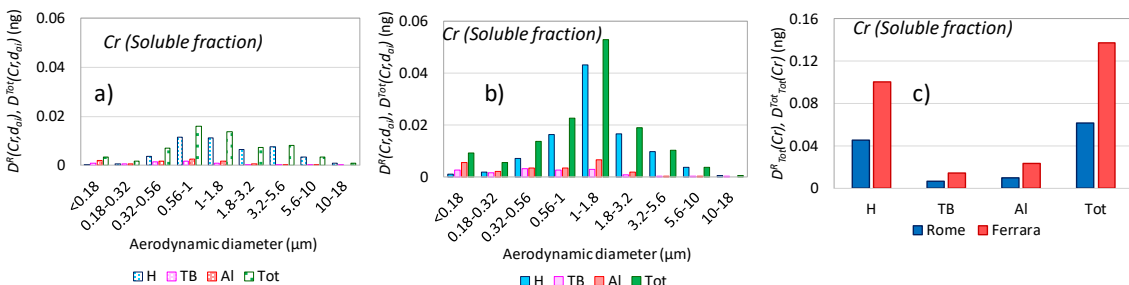


Figure S10. $D^R(Cr, d_{ai})$ and $D^{Tot}(Cr, d_{ai})$ doses at the Rome (a) and Ferrara (b) sites, relevant $D_{Tot}^R(Cr)$ and $D_{Tot}^{Tot}(Cr)$ doses (c) for Cr soluble fraction.

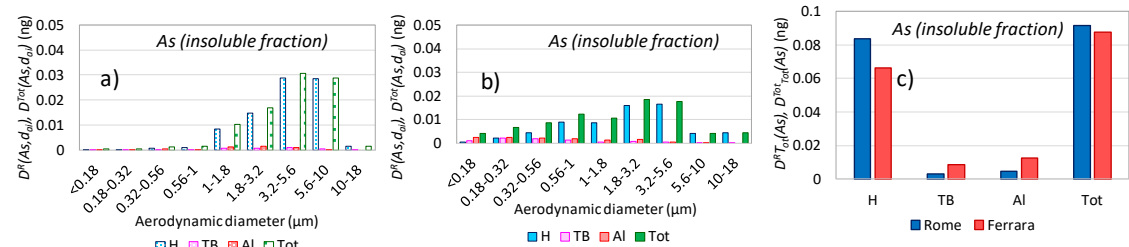


Figure S11. $D^R(As, d_{ai})$ and $D^{Tot}(As, d_{ai})$ doses at the Rome (a) and Ferrara (b) sites, relevant $D_{Tot}^R(As)$ and $D_{Tot}^{Tot}(As)$ doses (c) for As insoluble fraction.

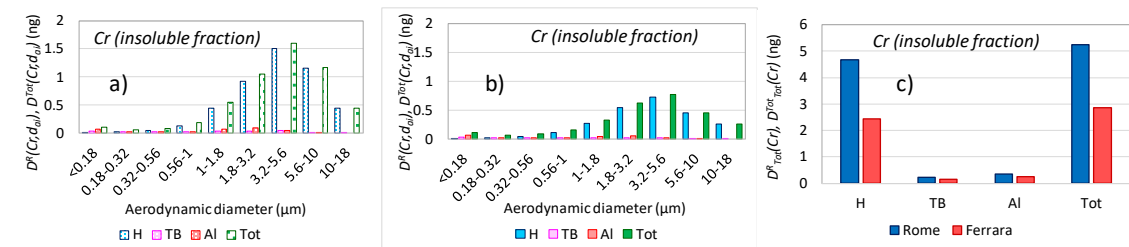


Figure S12. $D^R(Cr, d_{ai})$ and $D^{Tot}(Cr, d_{ai})$ doses at the Rome (a) and Ferrara (b) sites, relevant $D_{Tot}^R(Cr)$ and $D_{Tot}^{Tot}(Cr)$ doses (c) for Cr insoluble fraction.

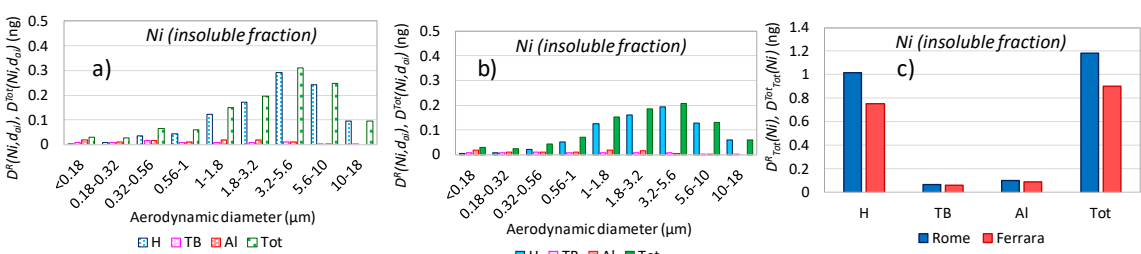


Figure S13. $D^R(Ni, d_{ai})$ and $D^{Tot}(Ni, d_{ai})$ doses at the Rome (a) and Ferrara (b) sites, relevant $D^R_{Tot}(Ni)$ and $D^{Tot}_{Tot}(Ni)$ doses (c) for Ni insoluble fraction.

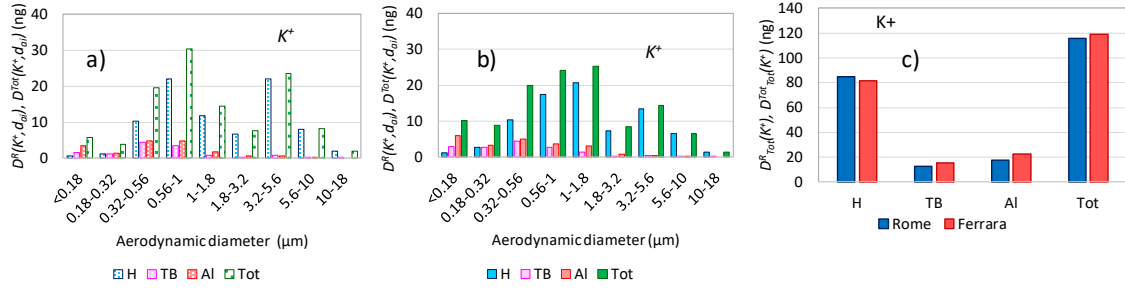


Figure S14. $D^R(K^+, d_{ai})$ and $D^{Tot}(K^+, d_{ai})$ doses at the Rome (a) and Ferrara (b) sites, relevant $D^R_{Tot}(K^+)$ and $D^{Tot}_{Tot}(K^+)$ doses (c).

Figure S1: $D^R(Sb, d_{ai})$ and $D^{Tot}(Sb, d_{ai})$ doses at the Rome (a) and Ferrara (b) sites, relevant $D^R_{Tot}(Sb)$ and $D^{Tot}_{Tot}(Sb)$ doses (c) for Sb insoluble fraction. Figure S2: $D^R(Cu, d_{ai})$ and $D^{Tot}(Cu, d_{ai})$ doses at the Rome (a) and Ferrara (b) sites, relevant $D^R_{Tot}(Cu)$ and $D^{Tot}_{Tot}(Cu)$ doses (c) for Cu soluble fraction. Figure S3: $D^R(Sb, d_{ai})$ and $D^{Tot}(Sb, d_{ai})$ doses at the Rome (a) and Ferrara (b) sites, relevant $D^R_{Tot}(Sb)$ and $D^{Tot}_{Tot}(Sb)$ doses (c) for Sb soluble fraction. Figure S4: $D^R(Al, d_{ai})$ and $D^{Tot}(Al, d_{ai})$ doses at the Rome (a) and Ferrara (b) sites, relevant $D^R_{Tot}(Al)$ and $D^{Tot}_{Tot}(Al)$ doses (c) for Al insoluble fraction. Figure S5: $D^R(Ce, d_{ai})$ and $D^{Tot}(Ce, d_{ai})$ doses at the Rome (a) and Ferrara (b) sites, relevant $D^R_{Tot}(Ce)$ and $D^{Tot}_{Tot}(Ce)$ doses (c) for Ce insoluble fraction. Figure S6: $D^R(Al, d_{ai})$ and $D^{Tot}(Al, d_{ai})$ doses at the Rome (a) and Ferrara (b) sites, relevant $D^R_{Tot}(Al)$ and $D^{Tot}_{Tot}(Al)$ doses (c) for Al soluble fraction. Figure S7: $D^R(Ti, d_{ai})$ and $D^{Tot}(Ti, d_{ai})$ doses at the Rome (a) and Ferrara (b) sites, relevant $D^R_{Tot}(Ti)$ and $D^{Tot}_{Tot}(Ti)$ doses (c) for Ti soluble fraction. Figure S8: $D^R(Ce, d_{ai})$ and $D^{Tot}(Ce, d_{ai})$ doses at the Rome (a) and Ferrara (b) sites, relevant $D^R_{Tot}(Ce)$ and $D^{Tot}_{Tot}(Ce)$ doses (c) for Ce soluble fraction. Figure S9: $D^R(Ni, d_{ai})$ and $D^{Tot}(Ni, d_{ai})$ doses at the Rome (a) and Ferrara (b) sites, relevant $D^R_{Tot}(Ni)$ and $D^{Tot}_{Tot}(Ni)$ doses (c) for Ni soluble fraction. Figure S10: $D^R(Cr, d_{ai})$ and $D^{Tot}(Cr, d_{ai})$ doses at the Rome (a) and Ferrara (b) sites, relevant $D^R_{Tot}(Cr)$ and $D^{Tot}_{Tot}(Cr)$ doses (c) for Cr soluble fraction. Figure S11: $D^R(As, d_{ai})$ and $D^{Tot}(As, d_{ai})$ doses at the Rome (a) and Ferrara (b) sites, relevant $D^R_{Tot}(As)$ and $D^{Tot}_{Tot}(As)$ doses (c) for As insoluble fraction. Figure S12: $D^R(Cr, d_{ai})$ and $D^{Tot}(Cr, d_{ai})$ doses at the Rome (a) and Ferrara (b) sites, relevant $D^R_{Tot}(Cr)$ and $D^{Tot}_{Tot}(Cr)$ doses (c) for Cr insoluble fraction. Figure S13: $D^R(Ni, d_{ai})$ and $D^{Tot}(Ni, d_{ai})$ doses at the Rome (a) and Ferrara (b) sites, relevant $D^R_{Tot}(Ni)$ and $D^{Tot}_{Tot}(Ni)$ doses (c) for Ni insoluble fraction. Figure S14: $D^R(K^+, d_{ai})$ and $D^{Tot}(K^+, d_{ai})$ doses at the Rome (a) and Ferrara (b) sites, relevant $D^R_{Tot}(K^+)$ and $D^{Tot}_{Tot}(K^+)$ doses (c).